IOP Publishing Journal of Physics: Condensed Matter

J. Phys.: Condens. Matter **23** (2011) 184122 (16pp) doi:10.1088/0953-8984/23/18/184122

Small-scale particle advection, manipulation and mixing: beyond the hydrodynamic scale

Arthur V Straube

Department of Physics, Humboldt University of Berlin, Newtonstraße 15, D-12489 Berlin, Germany

E-mail: straube@physik.hu-berlin.de

Received 22 July 2010, in final form 5 October 2010
Published 20 April 2011
Online at stacks.iop.org/JPhysCM/23/184122

Abstract

In this paper we discuss the problems of particle advection, manipulation and mixing at small scales. We start by considering reaction–advection–diffusion systems with the focus on mixing. We show how mixing advection affects the processes of reaction–diffusion and discuss mixing-induced instabilities. Further, we consider the problem of particle manipulation and discuss collective effects in systems comprising solid and compressible particles. We particularly discuss mechanisms of particle entrapment, the role of compressibility in the dynamics of bubbly liquids and nonequilibrium colloidal explosion. Finally, we address two issues related to the problem of wetting. First, we study the role of contact line motion for a sessile droplet (or a bubble) on an oscillating substrate. Second, we discuss an instability of a thin film leading to the formation of a fractal structure of droplets.

(Some figures in this article are in colour only in the electronic version)

1. Introduction: general aspects

The problems of particle advection, manipulation and mixing at small scales belong to the field of nano- and microfluidics, which is closely related to the concept of a lab-on-a-chip (LOC) [1]. Many of the techniques developed in the past 50 years promise cheaper and faster fabrication of LOC systems [2]. Nowadays applications [3] require understanding the dynamics of not only pure fluids but complex fluids such as colloidal suspensions, polymer solutions, microemulsions and reacting fluids. It is expected [4] that investigations of these complex systems will have a great impact in the biotechnological industry, pharmacology, medical diagnostics, environmental monitoring and basic research. Because of their structural complexity, complex fluids involve considerably different length scales and their description becomes a highly nontrivial task. Particular aspects of macro- and microworlds meet each other and become no longer separable at the intermediate scales [5, 6]. Understanding the mesoscopic dynamics of complex fluids including hydrodynamic and nonhydrodynamic interactions, effects of thermal noise, confinement and finite size, and especially their interplay, presents a major challenge for both theory and experiment [7, 8].

A typical and appealing example of a complex fluid is a fluid laden with colloidal particles, figure 1(a). Colloidal suspensions are interesting systems for many reasons. First, colloids are relatively slowly moving, which allows for precise and reliable experimental control and analyses [9]. Second, colloidal suspensions are universal model systems: their mutual intercolloidal interactions can be easily tuned, for example, by adding polymer coils or other colloidal particles. Third, there are at least two well-separated length scales in such systems: the size of the suspended particles and the size of the much smaller solvent molecules. The latter circumstance presents a major challenge from the theoretical point of view.

On the one hand, one could treat such a system from the perspective of continuum theory, assuming that it is applicable at small scales. In fluid dynamics, the problem of a single particle moving through a viscous fluid was solved by Stokes in his classical *tour de force* [10]. Here, the particle is considered to be macroscopic and the fluid is treated as a continuum. External forces exerted on particles lead to their motion. During the motion, each particle disturbs the fluid

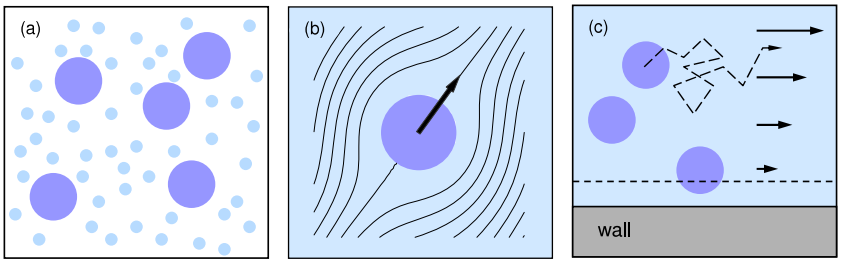

Figure 1. Different features of colloidal suspension at mesoscales. Colloids are plotted in dark blue, solvent (light blue) is represented as smaller particles or a coarse-grained continuum. (a) Colloidal suspension, discrete picture. (b) A moving colloidal particle disturbs the solvent and mediates long-range hydrodynamic interactions between the particles. (c) Brownian motion and the finite size of colloids in a driven solvent close to the wall. The colloid center can approach the wall up to a certain distance only (horizontal dashed line).

flow (see figure 1(b)) so that the velocity disturbance decays as $1/r$, where r is the distance measured from the particle. This indicates that moving particles are hydrodynamically coupled to each other via the solvent. Thus, even when the particles are not directly interacting, the viscous solvent mediates their indirect hydrodynamic interactions. One should keep in mind the long-range nature of hydrodynamic interactions, which generally causes a certain difficulty for the theoretical analysis of systems comprising many particles.

On the other hand, the colloidal particles are sufficiently small and experience the fluctuating thermal forces from the fluid, which gives rise to Brownian diffusion [11, 12], figure 1(c). Often, these inevitable effects of thermal noise are not properly taken into account in the continuum hydrodynamics. On the smallest microscopic level, which accounts for all the individual atomic interactions, such as, for example, in molecular dynamics (MD), the thermal noise effects are naturally included. Although the microscopic approaches are the most fundamental and ultimately the most precise, they have restrictions from the practical viewpoint. Being appropriate for pure fluid systems, the MD methods often become impracticable for complex fluids, which involve considerably different length scales, implying that systems of much larger size have to be simulated. Here, microscopic methods are still out of reach due to available computational power limiting the system size to about a few tens of nanometers.

Compared to the macroscopic scales, physics at smaller, intermediate scales can become significantly different. The role of boundaries (or more generally effects of confinement) becomes non-negligible or even predominant. The volume and surface mechanisms governing the dynamics scale as L^3 and L^2, respectively, where L is a characteristic length scale. Hence, the relative importance of surface effects increases as $1/L$, while the scale L is decreased. Another point is that the relative size of the particles becomes larger under confinement. The particles may have to be considered as having finite size, an important point that is often neglected in conventional approaches treating the particles as mathematical points. The finite size of particles can be of crucial importance in understanding the particle dynamics near confining walls, e.g. depletion effects [13]. In such a situation, the center of a finite size particle cannot approach the wall beyond a certain distance, which is typically equal to the radius of the particle (see figure 1(c)), whereas this zone is not forbidden for the solvent.

There are a number of other potentially important factors. For instance, particles in suspension interact with each other and with boundaries in many ways. Apart from the effects of hydrodynamic interactions, they can interact directly. This can be short-range repulsion, preventing each of two hard spheres from penetrating into each other or into the solid wall. Another generic case is the long-range interactions, e.g. attractive van der Waals forces or dipole–dipole interactions [14]. In the first case this can lead to attraction and therefore aggregation effects, while the second example depends on orientation of induced or true electric (or magnetic) dipoles and can lead to the formation of chains. Another typical situation is the case of dense suspensions, where the particle motion is effectively screened by other particles that are almost touching.

Rapid development of microtechnologies [4, 5] over the past few decades has attracted great interest in the theoretical aspects of wetting [15, 16]. This problem, where the surface forces prevail over the volume ones, involves understanding the dynamics of thin films (figure 2(a)) and is directly related to sessile droplet interaction with the substrate, see figure 2(b). A powerful approach to the thin film dynamics is based on the lubrication approximation [17]. Many studies have shown [17, 18] that the thin film can become unstable and rupture, leading to the formation of sessile droplets and complex cascades of droplets [19]. Note that, because the correct description of interaction with boundaries is a crucial prerequisite for obtaining the proper picture of the bulk dynamics in confined systems, a systematic understanding of the interaction of a single droplet with the substrate is able to shed light on the dynamics of systems illustrated in figures 1(c) and 2(c).

The presence of a solid surface faces another challenging problem underlying the physics of wetting, the contact line dynamics, which is currently far from being fully understood. Despite noticeable progress in the theoretical understanding of the physics of a steadily moving contact line [15, 20], the unsteady motion of the contact line remains significantly less explored, especially for fast oscillatory processes. Of special importance is the role of contact angle hysteresis. Based on Dussan's experiments [21], a boundary condition that captures principal features of the contact line motion has been suggested by Hocking: with [22] and without [23] hysteresis. Different

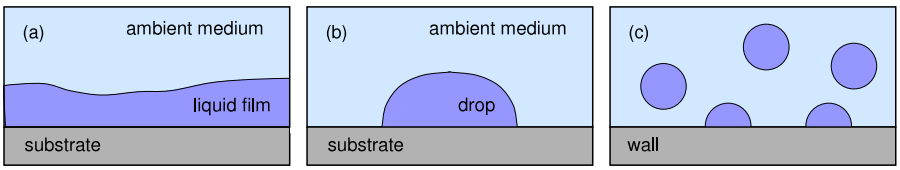

Figure 2. Systems under consideration. (a) Thin film spreading over a solid surface. (b) A drop sitting on the surface. Such drops can appear as a result of thin film rupture. (c) Disperse medium comprising the drops (bubbles), a part of which sit on the wall and the others are suspended in the bulk.

practically important situations are addressed by changing a wetting parameter and range from the completely pinned contact line (the contact angle changes) to the opposite case of the fixed contact angle (the contact line moves). For sessile oscillating drops and bubbles most theoretical studies apply oversimplified models, when hysteretic phenomena [24, 25] or the contact line motion [26] are neglected. As a result, principal questions referring to the dynamics of the contact line remain unsolved. For instance, recent experiments [27] have detected stick–slip motion, which cannot be satisfactory described by the oversimplified models [28].

In this paper, we discuss three closely related issues. In section 2, we consider chemical and biochemical systems in terms of reaction–advection–diffusion systems and focus on the role of mixing. We demonstrate that mixing flows can have a significant impact on the dynamics of these systems and lead to a number of novel instabilities. In section 3 we deal with the problem of particle manipulation. We consider different effects of collective behavior and discuss how such effects can be described in a consistent and efficient way. In particular, we discuss the mechanism of particle entrapment and then focus on the dynamics of bubbles as soft particles. We show that the compressibility of bubbles can lead to a number of peculiar effects. Finally, in section 4, we survey two issues related to the problem of wetting. First, we consider the dynamics of fast oscillatory motion, which is studied in the context of a sessile droplet (or a bubble) on an oscillating substrate. Second, we discuss an instability of a thin film and show how a complex hierarchical structure of droplets develops as a result of thin film rupture.

2. Dynamics of chemical and biochemical systems and mixing

When the chemical species suspended in a fluid solvent have a typical size comparable with that of the solvent, there is no significant separation of length scales and the systems can be efficiently described by means of the continuum theory. Reaction–diffusion systems are a well-established class of continuum models describing pattern formation far from equilibrium [29]. Often, pattern-forming fields are additionally transported by fluid flows. Various examples range from macroscopic plankton patterns in oceanic flow [30, 31] to chemical reactions in microchannels [32]. By incorporating the flow in the model one arrives at reaction–advection–diffusion systems. The spatiotemporal evolution of concentrations C_j $(j = 1, \ldots, N)$ can be described by the following equations [33, 34]:

$$\frac{\partial C_j}{\partial t} + \mathbf{v} \cdot \nabla C_j = D_j \nabla^2 C_j + F_j(C_1, \ldots, C_N). \quad (1)$$

Here, $\mathbf{v}(\mathbf{r}, t)$ is the velocity field, which is assumed to be solenoidal ($\nabla \cdot \mathbf{v} = 0$), D_j are the molecular diffusivities of the corresponding chemical species and functions F_j describe reaction kinetics.

A great variety of chemical and biochemical processes in closed and open flow geometries can be described in terms of the model (1). We note, however, that this model implies that the velocity field is not affected by the chemical species so that $\mathbf{v}(\mathbf{r}, t)$ is independent of C_j. Although this assumption greatly simplifies the analysis and is often reasonable for small volume concentrations, it is not always true, especially for systems in external fields. In section 3 we provide a number of examples where such a feedback of particles onto the flow can be important even when the volume concentration of an admixture is small. Apart from the assumption of being divergence-free, the velocity field $\mathbf{v}(\mathbf{r}, t)$ in equation (1) can be rather arbitrary. Further, we are interested in understanding the role of mixing and therefore focus on mixing flows [35–37].

A typical experimental implementation of a two-dimensional mixing flow $\mathbf{v}(\mathbf{r}, t)$ is a closed flow periodic in space and time [38]. Qualitative features of mixing can be captured by a model two-dimensional flow that is 2π-periodic in space. As suggested by Antonsen *et al* [39] (see also a closely related study [40]), the velocity field can be represented as follows:

$$\mathbf{v} = \mathbf{e}_x U_x f(t) \sin[y + \theta_x(t)] + \mathbf{e}_y U_y [1 - f(t)] \sin[x + \theta_y(t)]. \quad (2)$$

The function $f(t)$ describes switching between two shear flows in x and y directions with the amplitudes U_x and U_y. Depending on functions $f(t)$, $\theta_x(t)$, $\theta_y(t)$, the flow can be time periodic or irregular. A weakly turbulent irregular flow is modeled by choosing $f(t), \theta_x(t), \theta_y(t)$ to be random functions of time. For a time periodic flow, one sets θ_x, θ_y to be constant and

$$f(t) = \begin{cases} 1, & 0 < t < T/2, \\ 0, & T/2 < t < T \end{cases} \quad (3)$$

with T being the time period. In this case, particle trajectories demonstrate typical Hamiltonian dynamics with both regular and chaotic orbits. Thus, the phase space is mixed, comprising the stability islands and chaotic regions. An advantage of the time periodic flow (2) and (3) is that the trajectories of particles can be obtained explicitly. The transformation of

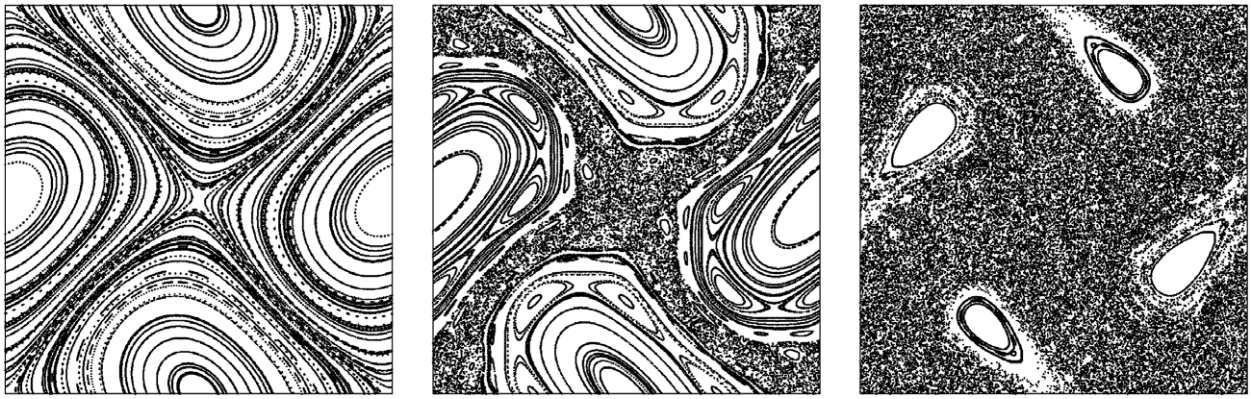

Figure 3. Phase portraits of the mapping (4) and (5) for a periodic driving, $T = 1$, $\theta_x = \theta_y = 0$. The parameters $U_x = U_y = 1.5$ (a), $U_x = U_y = 3.0$ (b) and $U_x = U_y = 5.0$ (c).

particle coordinates during one period T is given by an area-preserving mapping:

$$x(t+T) = x(t) + \tfrac{1}{2}U_x T \sin[y(t) + \theta_x], \tag{4}$$

$$y(t+T) = y(t) + \tfrac{1}{2}U_y T \sin[x(t+T) + \theta_y]. \tag{5}$$

The phase space dynamics of mapping (4) and (5) restricted to the domain of periodicity $x, y \in [0, 2\pi]$ is demonstrated in figure 3. We see that the phase space consists of regular islands and domains of chaotic behavior. With the growth in advection rate (U_x, U_y), the domains of the quasiperiodic dynamics are gradually superseded by the chaotic regions. Generally, the angles θ_x and θ_y can take on different values in each time period. For instance, for θ_x and θ_y constant in each period but varying randomly from period to period, all the trajectories are chaotic.

As has been shown experimentally in a nonreactive set-up ($F_j = 0$), a dye subject to chaotic advection in a fluid can form persistent patterns [38]. The described model of mixing flow (4) and (5) has been recently applied to explain these long-living patterns [41]. Further, we overview a few examples involving closed and open reactive flows and showing novel instabilities in reaction–advection–diffusion systems where mixing plays an important role.

2.1. Temporal chaos versus spatial mixing

We first focus on a reaction–advection–diffusion system (1) with a time-dependent reaction [42]. The system is considered in a closed domain with the no-flux boundary conditions $\nabla C_j|_S = 0$ at the boundary S. Note that, for a spatially homogeneous distribution of concentrations, the advection and diffusion terms vanish. Model (1) is reduced to a nonlinear system

$$\frac{\mathrm{d}C_j}{\mathrm{d}t} = F_j(C_1, \ldots, C_N), \tag{6}$$

which admits temporally regular or chaotic solutions $C_j^0(t)$. The question arises as to whether the spatially homogeneous state $C_j^0(t)$ can become unstable and the transition to a spatially inhomogeneous state can take place. To answer this question, we introduce a small perturbation field $\varphi_j(\mathbf{r}, t)$ of the concentration, substitute the perturbed field $C_j^0(t) + \varphi_j(\mathbf{r}, t)$ into equation (1) and linearize it near the solution $C_j^0(t)$. By measuring the time in the scale of the characteristic advection time, we arrive at dimensionless equations for perturbations:

$$\frac{\partial \varphi_j}{\partial t} + \mathbf{v} \cdot \nabla \varphi_j = d_j \nabla^2 \varphi_j + Da J_{jk} \varphi_k, \tag{7}$$

where $J_{jk}(t) = (\partial F_j / \partial C_k)$ is the Jacobian matrix of equation (6) taken on the solution $(C_1^0(t), \ldots, C_N^0(t))$. The dimensionless diffusion constants d_j, which are equivalent to Péclet numbers $Pe_j \sim d_j^{-1}$ and are generally distinct for different species, set the relative intensity of diffusion relative to advection at the characteristic length scale. The Damköhler number Da is the dimensionless reaction rate.

Generally, the solutions of (7) grow or decay exponentially in time $||\varphi|| \sim \mathrm{e}^{\lambda t}$, where λ belongs to the spectrum of Lyapunov exponents (LE). Note that the LEs of the solution of (6) belong to this spectrum, describing growth or decay of homogeneous perturbations. The stability of the spatially homogeneous solution $C_j^0(t)$ towards inhomogeneous perturbations is described by the largest LE corresponding to a spatially varying Lyapunov vector $\varphi(\mathbf{r}, t)$—the transverse LE $\lambda_\perp$ (in the sense that it is transverse to a manifold of spatially homogeneous solutions of (7)). Generally, for different diffusion constants and a given time-dependent flow $\mathbf{v}(\mathbf{r}, t)$, the transverse LE can be determined only numerically. However, we show that an analytic solution obtained for a simple situation works well for other possible set-ups.

In the simplest case of a time-independent velocity field $\mathbf{v} = \mathbf{v}(\mathbf{r})$ and equal diffusion constants $d_j = d$, an analytic expression for the transverse LE, $\lambda_\perp$, can be obtained. In this case, the time and space dependences in equation (7) can be separated by putting $\varphi_j(\mathbf{r}, t) = X(\mathbf{r})\Phi_j(t)$. As a result [42], we find $\Phi_j \sim \exp(\lambda_\perp t)$ with

$$\lambda_\perp = Da \cdot \lambda - \gamma(Pe), \tag{8}$$

where λ is the largest LE of the attractor in equation (6) and γ is the smallest nonvanishing eigenvalue of an advection–diffusion eigenvalue problem, which is not required to

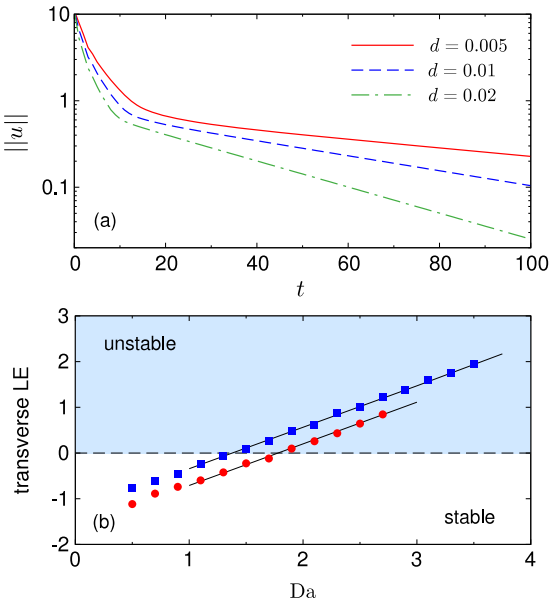

Figure 4. (a) Example showing the behavior of $||u||$ with time evaluated for different d and a time periodic $\mathbf{v}(\mathbf{r}, t)$ as in equation (2). The slope of the curves provides γ. (b) Numerical evaluation of $\lambda_\perp$ from equation (7) (markers) and from approximations like in equation (8) (lines). The chaotic reaction is modeled via the Lorenz model ($N = 3$), the flow field (2) is chosen to be irregular, as described in the main text, $U_x = U_y = 20$, $\langle T_{\text{int}} \rangle = 0.5$. Squares correspond to $d_i = 0.1$, circles: $d_1 = 0.1$, $d_2 = 0.2$, $d_3 = 0.5$.

be solved explicitly. Instead, we follow another way of determining γ, which is applicable for an arbitrary time-dependent flow. The value γ can be interpreted as the asymptotic decay rate of the contrast of a passive scalar $u(\mathbf{r}, t)$ in the advection–diffusion problem, see also figure 4(a):

$$\frac{\partial u}{\partial t} + \mathbf{v} \cdot \nabla u = d\nabla^2 u \tag{9}$$

and evaluated in the sense of the LE:

$$\gamma = -\lim_{t\to\infty} \frac{\ln ||u(\mathbf{r}, t)||}{t}. \tag{10}$$

As follows from equation (8), the stability condition of the spatially homogeneous state corresponds to $\lambda_\perp < 0$. If the oscillations of the concentrations are regular, then the largest LE is nonpositive, $\lambda \leqslant 0$, and this regime is always stable against spatially inhomogeneous perturbations. A nontrivial transition occurs for chaotic reactions, if $\lambda > 0$. Here the stability condition leads to the critical value

$$Da_{\text{cr}} = \frac{\gamma(Pe)}{\lambda}. \tag{11}$$

A similar condition for a trivial case of a reaction–diffusion system has been obtained in [43] and for an abstract mapping model of mixing in [44].

Following these ideas, we have evaluated γ for a time-dependent flow (2), see figure 4(a). The value of γ depends crucially on the nature of the flow and hence the Péclet number, which is consistent with a previous study [41]. Note that result (8) can be generalized for the case of different diffusion constants, including weakly turbulent irregular flows [42]. To model weakly turbulent flows, we applied flow (2) with $f(t)$ being a $(0, 1)$-telegraph process with independent exponentially distributed time intervals T_{int} and independent uniformly distributed phases θ_x, $\theta_y \in (0, 2\pi)$. An example of the transverse LE is shown in figure 4(b). Remarkably, $\lambda_\perp$ is nearly a linear function of Da, similar to that in equation (8). This observation strongly suggests that the transition to spatially inhomogeneous structures in a mixed flow with chaotic in time reaction is determined by the transverse LE, which can be effectively represented by a sum of competing contributions. One is destabilizing and is caused by temporal chaos in the reaction, while another is stabilizing and comes from spatial mixing. It is noteworthy that these two tendencies remain essentially 'separable' for all set-ups considered. The stability threshold is in agreement with the numerical simulations of the full nonlinear model.

2.2. *Advection-induced instability*

A variety of situations in biological and chemical contexts can be described by the dynamics of a pair of interacting species—an activator and an inhibitor. A popular chemical model is the Brusselator [45] or its modifications. For spatially distributed fields, apart from reaction the dynamics involves diffusion (molecular diffusion for chemical systems or irregular mobility in biological applications) and advection, as described by equation (1) with $N = 2$ species: $j = 1$, say, an activator, and $j = 2$, an inhibitor. As was mentioned in section 2.1, equation (1) admits a spatially homogeneous state and, in particular, a (constant) steady state, C_j^0.

As has been shown recently, a simple shear flow is able to destabilize such a spatially homogeneous state [46]. A reasonable question to ask is whether a similar destabilization effect can be found for mixing flows. One might intuitively expect that, as mixing smears spatial nonuniformities, it results in stabilization of a spatially homogeneous state, as happens, for instance, for chaotic reactions [42], section 2.1. Here, we address this question for a general two-dimensional reaction–diffusion system capable of Turing instability [47] and demonstrate that instability can be induced by an advection of one component of the reaction [48].

As earlier, normalizing time by the advection time and denoting by $\varphi_1(\mathbf{r}, t)$ and $\varphi_2(\mathbf{r}, t)$ the small deviations from the steady state concentrations C_1^0 and C_2^0, we arrive at a linear reaction–advection–diffusion system for perturbations:

$$\frac{\partial \varphi_1}{\partial t} + \mathbf{v} \cdot \nabla \varphi_1 = d_1 \nabla^2 \varphi_1 + a\varphi_1 + b\varphi_2, \tag{12}$$

$$\frac{\partial \varphi_2}{\partial t} + \mathbf{v} \cdot \nabla \varphi_2 = d_2 \nabla^2 \varphi_2 + c\varphi_1 + d\varphi_2. \tag{13}$$

Here, the mixing flow field $\mathbf{v}(\mathbf{r}, t)$ is given via equation (2), d_1 and d_2 are diffusivities of the activator and inhibitor, respectively, and a, b, c, d are parameters of the kinetics. In the absence of advection the problem reduces to the classical reaction–diffusion model (see, e.g., [49]), where two principal instabilities are a spatially homogeneous Hopf bifurcation and

a Turing instability. Our main interest is in the case where Turing instability is dominant, which is ensured by setting $d_1 < d_2$.

Although the flow $\mathbf{v}(\mathbf{r}, t)$ is periodic in space, the fields $\varphi_j(\mathbf{r}, t)$ do not have to be periodic. A general perturbation should be taken in the Bloch form:

$$\varphi_j(x, y, t) = \mathrm{e}^{\mathrm{i}\kappa_x x + \mathrm{i}\kappa_y y}\Phi_j(x, y, t), \tag{14}$$

where Φ_j are now 2π-periodic functions in x and y and additional parameters κ_x, κ_y stand for quasimomenta. Since the exponential factor in equation (14) has a period of 1 with respect to κ_x and κ_y, we consider a symmetric interval of independent values κ_x, $\kappa_y \in [-0.5, 0.5]$. Then, because of periodicity of Φ_j, the solutions can be represented as Fourier series:

$$\Phi_j(x, y, t) = \sum_{l,m} \phi_{lm}^{(j)}(t)\,\mathrm{e}^{\mathrm{i}(lx+my)}. \tag{15}$$

Afterwards, the method of transverse LE can be applied to perform the linear stability analysis. Using the advantage of the flow model, where we choose $T = 1$, $\theta_x = \theta_y = 0$, $U_x = U_y = U$, we can apply a discrete-in-time model. Within each time interval T the scalar fields φ_j evolve in three stages, corresponding to advection, diffusion and reaction. These subprocesses act as successive operators $\hat{L}_\mathrm{A}$, $\hat{L}_\mathrm{D}$ and $\hat{L}_\mathrm{R}$, whose product provides a reaction–advection–diffusion propagator over one time interval: in the Fourier space we have $\phi_{lm}^{(j)}(t+T) = \hat{L}_\mathrm{R}\hat{L}_\mathrm{D}\hat{L}_\mathrm{A}\phi_{lm}^{(j)}(t)$. The advection $\hat{L}_\mathrm{A}$ and diffusion $\hat{L}_\mathrm{D}$ operators are given via

$$\hat{L}_\mathrm{A}\phi_{lm}^{(j)} \to \sum_{p,q} J_{q-m}[(p+\kappa_x)UT/2] \times J_{p-l}[(m+\kappa_y)UT/2]\,\phi_{pq}^{(j)},$$

$$\hat{L}_D\phi_{lm}^{(j)} \to \mathrm{e}^{-[(l+\kappa_x)^2+(m+\kappa_y)^2]d_jT}\phi_{lm}^{(j)}.$$

The reaction operator couples the species, $\phi_{lm}^{(j)} \to \sum_k(\hat{L}_\mathrm{R})_{jk}\,\phi_{lm}^{(k)}$, $\hat{L}_\mathrm{R} = \hat{R}/(\Lambda_- - \Lambda_+)$, where $\hat{R}$ is given by elements

$$\hat{R} = \begin{pmatrix} \Lambda_- E_+ - \Lambda_+ E_- & b(E_- - E_+) \\ \frac{\Lambda_-\Lambda_+(E_+ - E_-)}{b} & \Lambda_- E_- - \Lambda_+ E_+ \end{pmatrix}.$$

Here, $E_\pm = \exp(\lambda_\pm T)$, $\Lambda_\pm = \lambda_\pm - a$ and

$$\lambda_\pm = \frac{a+d}{2} \pm \frac{\sqrt{(a-d)^2 + 4bc}}{2},$$

which are assumed to be real, in accordance with our choice of the absence of the Hopf bifurcation. This discrete time approach enormously simplifies the calculations, while yielding a quantitatively correct picture of the process.

To some extent, the influence of advection in an advection–diffusion system can be understood from the idea of effective diffusion: mixing effectively increases the diffusion constant. Therefore one can expect that the dynamics of a reaction–advection–diffusion system is similar to that of a reaction–diffusion system with larger diffusion constants. More importantly, in the system under consideration there are two coupled species and the Turing instability is caused by a difference in diffusivities of the species. Although advection can effectively change the diffusion constants of the species, it is not clear how this difference will be affected by advection. However, the situation becomes much more transparent if only one species is advected. Then, an advection, contributing to its effective diffusion, may increase or decrease the difference of diffusion constants, thus enhancing or suppressing the instability.

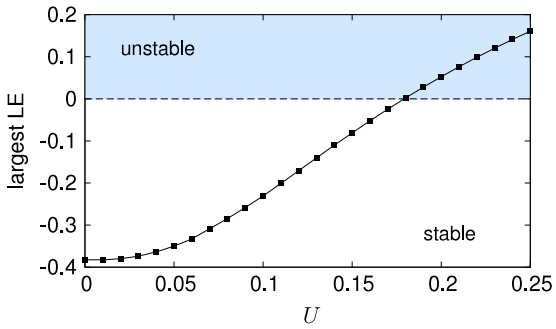

Figure 5. Largest LE as a function of advection rate, U. The parameters are $a = 5.35$, $c = -6.35$ and $\kappa_x = \kappa_y = 0.5$.

Below we focus on a situation when only one species, namely that of higher diffusivity, is advected. We set the parameters $b = 8$, $d = -9$, $d_1 = 0.0025$ and $d_2 = 0.0075$. So, we assume that the mobility of the 'activator' φ_1 is relatively low, and it is not advected at all. Following the described mapping approach, we apply the usual method for estimation of the largest LE of mappings, see, e.g., [41]. We choose the parameters of the reaction in such a way that the homogeneous solution is stable in the absence of advection, and then switch on mixing of the inhibitor, $\varphi_2(\mathbf{r}, t)$. The dependence of the largest LE on the advection rate is presented in figure 5. We detect the growth of the largest LE, which becomes positive at $U_\mathrm{cr} \approx 0.18$. So, this example shows clearly that mixing can play a destabilizing role.

Remarkably, the quasimomenta in the Bloch ansatz (14) are essential in the stability analysis. Below we present three examples where mostly unstable modes correspond to different values of quasimomenta. In figure 6 we show the corresponding patterns close to the stability threshold. In the first case, $\kappa_x = \kappa_y = \pm 0.5$, which indicates that the unstable patterns have a 'chessboard' structure with respect to the periodicity of the original flow. The pattern in figure 6(b) corresponds to $\kappa_x = \kappa_y = 0$, with the periodicity of the pattern the same as the periodicity of the imposed flow. The last pattern, figure 6(c), shows the case of $\kappa_x = 0$, $\kappa_y = \pm 0.4$, where the periodicities of the patterns in the x and y directions are not the same and are not identical to the periodicity of the flow. We note that these are linear modes, which are expected to describe the overall picture close to the stability threshold. Away from the threshold the full nonlinear model should be applied.

Thus, this example shows that a mixing advection of one of the species may destabilize the spatially homogeneous state, leading to a pattern-forming instability. Physically, this can be explained as crossing a threshold of Turing instability due to an effective increase of one of the diffusion constants.

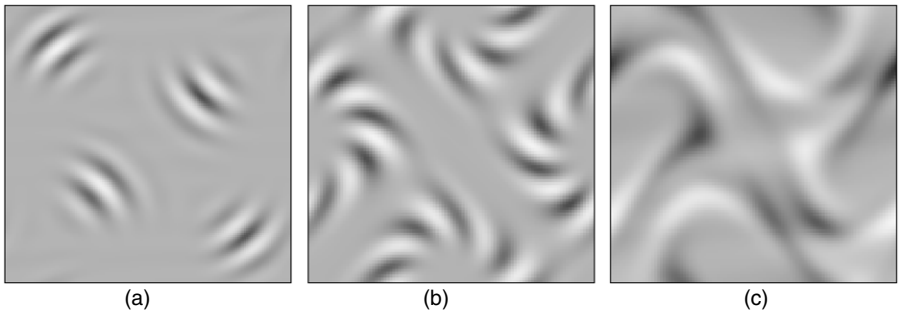

Figure 6. Patterns close to the threshold for different parameters. (a) $a = 5.35$, $c = -6.35$, $U = 0.18$, $\kappa_x = \pm 0.5$, $\kappa_y = \pm 0.5$; (b) $a = 3.7$, $c = -4.7$, $U = 0.77$, $\kappa_x = 0$, $\kappa_y = 0$ and (c) $a = 3.1$, $c = -4.1$, $U = 3.5$, $\kappa_x = 0$, $\kappa_y = \pm 0.4$ (and similarly for $\kappa_x = \pm 0.4$, $\kappa_y = 0$).

2.3. Mixing-induced global modes in open active flow

In sections 2.1 and 2.2 we discussed the role of mixing in reaction–advection–diffusion systems in the context of closed flows. In many natural and laboratory flows active chemical and biological processes occur in an open rather than in a closed geometry. Examples include chemical reactions in micromixers and plankton growth in oceans, see, for example, [34] and references therein. Here, 'activity' means that a chemical or biological species grows in time and the main issue is whether the throughflow is stronger or weaker than the activity. One has to compare the velocity of the throughflow with the velocity of the activity spreading due to diffusion [50]. If the throughflow is stronger, the activity is 'blown away' like a candle flame in a strong wind, in the opposite case a sustained activity can be observed [51, 52]. This simple picture is valid, however, only for homogeneous media. Often additional vortices are superimposed on a constant throughflow, due to, for example, mixing enforced by revolving fan blades in laboratory experiments or wakes behind islands in ocean currents. Here we discuss under which conditions such an additional kinematic mixing in a strong open flow can lead to a transition to a sustained activity and characterize this transition quantitatively.

We focus on a reaction–advection–diffusion system, equation (1), with a single species, $N = 1$, only. The dimensionless concentration of an active scalar field $C(\mathbf{r}, t)$ evolves according to

$$\frac{\partial C}{\partial t} + (\mathbf{V} + \mathbf{W}(\mathbf{r}, t)) \cdot \nabla C = d_0 \nabla^2 C + aC(1 - C^p), \quad (16)$$

where $\mathbf{V} = (V, 0, 0)$ is a constant throughflow in the x direction and d_0 is a molecular diffusion of the scalar field. Activity is assumed to be of the simplest form: a linear growth with rate a with a saturation at $C = 1$. The nonlinearity index p is typically an integer (1 or 2) for chemical reactions, while for biological populations a wide range of values of p has been recently reported [53]. Mixing is described by a spatially localized incompressible velocity field $\mathbf{W}(\mathbf{r}, t)$, where its intensity is denoted as W. Note that in the absence of fluid flow equation (16) is reduced to the famous Kolmogorov–Petrovsky–Piskunov–Fisher (KPPF) model of an active medium with diffusion (see, e.g., [54] for original references, analysis and applications of KPPF), while for $a = 0$ equation (16) describes a linear evolution of a passive scalar in a flow. Model (16) can be used for the description of biological activity. Here C plays the role of concentration of a growing bacterial population [55] subject to both turbulence and uniform drift because of the ability to swim in a particular direction. This model is also suitable for active flows in a microchannel, see figure 7(a); for a possible laboratory implementation see recent experiments with an autocatalytic reaction in a Hele-Shaw cell with a throughflow [32].

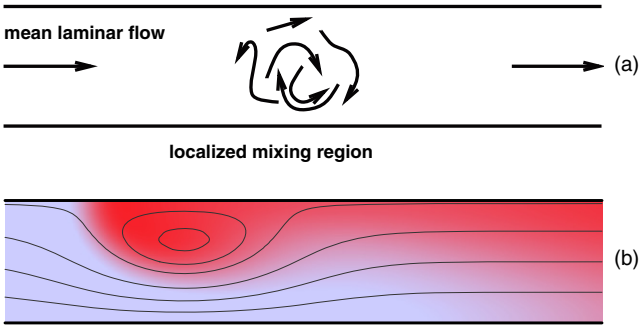

Figure 7. (a) Sketch of a micropipette with an open active flow comprising a mean laminar throughflow $\mathbf{V}$ and a localized mixing flow $\mathbf{W}$. (b) Example of the global mode in a model open flow with a vortex in a micropipette. The lower and higher values of the active scalar C correspond to lighter (light blue) and darker (red) domains, respectively.

In the absence of flow, the diffusion causes the active state to spread, forming eventually a front with velocity $V_f = 2\sqrt{ad_0}$ [50]. Thus, for vanishing mixing $W = 0$, the activity is blown away provided $V > V_f$. For this parameter range the instability in equation (16) is convective and, in the absence of external sources, no activity is observed in the medium. A nontrivial state is, however, possible if a localized mixing $\mathbf{W}(\mathbf{r}, t)$ is introduced into the flow [56, 57]. Beyond some critical intensity W_{cr}, the mixing turns the convective instability locally into the absolute one, which results in a nontrivial self-sustained distribution of C, which is referred to as the global mode, see figure 7(b).

The birth of the mixing-induced self-sustained structure can be understood if the concept of effective diffusion (see, e.g., [58]) is used to describe the mixing term in equation (16).

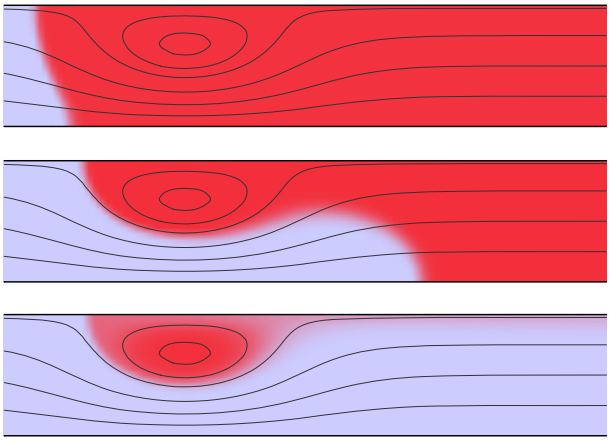

Figure 8. Entrapment of a passive scalar field in an open flow with a vortex. The initial state corresponds to the uniform distribution of the field. Panels (a), (b) and (c) show distributions of the scalar field at the beginning of evolution and at later times, respectively. The diffusivity is chosen to be relatively small such that the characteristic diffusion time is much larger than the advection time. A long-living structure in the form of a cloud (c) evolves from the initial state. The color code is as in figure 7.

In this approach, an effective diffusivity $d(\mathbf{r}) = d_0 + d_{\mathrm{mix}}(\mathbf{r})$, which accounts for the coarse-grained mixing dynamics. Clearly, a hump of diffusivity $d(\mathbf{r})$ leads to an increase of the local front velocity V_{f}, and one expects that, when the front propagation prevails over the throughflow, a stationary global mode can appear, producing a mixing-induced sustained structure. On the other hand, the role of a mixing vortex can be easily understood in a different way. In the case of a passive advection–diffusion process, $a = 0$, equation (16) is reduced to equation (9) with the flow field:

$$\mathbf{v} = \mathbf{V} + \mathbf{W}. \tag{17}$$

For a relatively small molecular diffusivity, passive particles are trapped by the vortex. In the limit of vanishing diffusivity, all the particles outside the vortex are blown away, i.e., in such domains their concentration $C = 0$, whereas the particles inside the vortex are trapped in a 'cloud' and can never escape, [59], see figure 8 and also section 3.1. Of course, for a nonvanishing d the concentration of particles in the cloud will gradually decrease. However, the particles under consideration represent the chemical or biological species, meaning that their concentration grows in time. For the particles trapped in the cloud, this temporal growth can compensate for the loss caused by diffusion. As a result, a self-sustained pattern is born, see figure 7(b).

Thus, this qualitative picture shows that, beyond the criticality, $W > W_{\mathrm{cr}}$, the mixing region acts as an effective source of the field; for an alternative and more rigorous discussion, see [56]. As can be shown, behind the source, an exponentially growing 'tail' extends downstream and then saturates to the value $C = 1$, forming a 'plateau', see figure 7(b). The intensity of the effective source ϵ_{eff} is shown to obey a universal scaling law [56, 57]: $\epsilon_{\mathrm{eff}} \sim (W - W_{\mathrm{cr}})^{\beta}$. The critical index β depends only on the nonlinearity index p and on the dimensionless velocity $v = V/V_{\mathrm{f}}$:

$$\beta = \begin{cases} p^{-1} & \text{if } v > \frac{2+p}{2\sqrt{1+p}}, \\ \dfrac{v - \sqrt{v^2-1}}{2\sqrt{v^2-1}} & \text{if } 1 < v < \frac{2+p}{2\sqrt{1+p}}. \end{cases} \tag{18}$$

The exponent β is determined solely by the nonlinearity index p if the throughflow velocity is much larger than the front velocity (v large). Here the field in the plateau domain is effectively uncoupled from the source and the saturation of the instability is due to the local nonlinearity at the source. For a small throughflow velocity (v close to one) the plateau state interacts with the source via the tail. Due to this coupling, the field at the source is saturated more efficiently than due to nonlinearity; here the exponent β is determined solely by the form of the tail, which depends on the velocities ratio v. Notably, although obtained from a one-dimensional consideration within the framework of the effective diffusivity approximation, the prediction (18) is in good quantitative agreement with numerical calculations of the full model (16), including one- and two-dimensional geometries and time-dependent flows.

3. Small-scale particle advection and particle manipulation

Motivated by numerous applications in medicine, biotechnology and pharmaceutical research, single and collective particle manipulation is an important problem of micro- and nanofluidics [4, 5]. The particles can be colloids, liquid droplets, small bubbles, macromolecules, cells or microorganisms, which can be manipulated directly, via dielectrophoretic [60], magnetic [61–63] or acoustic [64] forces and optical tweezers [65], or indirectly, via colloidal microdevices such as pumps and valves [66, 67]. Currently, no universally preferable technique exists, as all the means have their own advantages and restrictions. For soft objects and compressible media, time-alternating fields become promising. The fact that soft objects can change their shape and/or volume (cells [68], bubbles [69]) can provide an additional 'degree of freedom', which can be used to exert time-averaged forces on the particles and therefore manipulate soft objects. For bubbly liquids [70, 71], compressibility is often the major factor determining the dynamics of the medium.

An efficient description of a large number of particles in a fluid environment can be achieved via continuum theory, by looking at the spatiotemporal dynamics of concentration fields, as in section 2. Compared to biochemical processes, here we are interested in 'passive' processes, which involve no biological or chemical transformations (or reactions) of concentration fields. On the other hand, manipulation implies the existence of external forces exerted on the particles. Under the action of external forces particle move and, as mentioned in section 1, disturb the solvent and, hence, change the fluid velocity field. This effect is referred to as particle feedback. It is conventionally assumed that particle feedback can be neglected provided that the volume concentration of particles is small. We emphasize that, if the intensity of the external

field is high enough, it is often no longer appropriate to neglect particle feedback effects, which is true even for small volume concentrations. Below we provide a few examples demonstrating the importance of such effects.

3.1. Particle entrapment at small scales and particle feedback

The conventional mechanism of particle entrapment has been known for a long time [72]. Consider particles carried by a laminar vortex flow $\mathbf{W}$ and let a uniform external force, say, gravity, be exerted on the particles. If the inertia of particles is insignificant, the dimensionless velocity of particles can be presented as [73]

$$\mathbf{v} = S\mathbf{e}_x + \mathbf{W}. \tag{19}$$

Here, the first term is the sedimentation velocity characterized by a dimensionless parameter $S \propto g$ with $\mathbf{g} = g\mathbf{e}_x$ the gravity acceleration and $\mathbf{e}_x$ the unit vector along the gravity. Note that this term is equivalent to the constant throughflow $\mathbf{V}$ as in section 2.3 and velocity representation (19) for $\mathbf{v}$ becomes the same as in equation (17).

Consider now a suspension of particles with an initially uniform distribution, $C(\mathbf{r}, t = 0) = C_0$, and let it evolve in the flow field (19) [59]. To be precise, $C(\mathbf{r}, t)$ has the meaning of the volume fraction of particles. However, for the sake of simplicity we will call it concentration, as they differ by a constant factor only. For a negligible diffusion, the evolution of particle concentration corresponds to a purely advective transport:

$$\frac{\partial C}{\partial t} + \mathbf{v} \cdot \nabla C = 0. \tag{20}$$

In the case of no background vortex, $\mathbf{W} = 0$, the particle velocity field $\mathbf{v} = S\mathbf{e}_x$. Particle trajectories, which correspond to the streamlines of the flow field (19), are straight vertical lines. All the particles sediment along these lines and no entrapment is possible. If $\mathbf{W} \neq 0$ but the vortical motion is relatively weak compared with sedimentation, particle trajectories start to bend but particles are still not trapped, see figure 9(a). If the intensity of vortex flow is increased, particle entrapment becomes possible, as there appear closed orbits separated from non-closed trajectories by a separatrix loop, figure 9(b). The separatrix loop forms the boundary of the cloud of trapped particles. Inside the loop, the particles move along the closed orbits and therefore cannot escape, whereas all other particles eventually leave the system. This situation is similar to the case presented in figure 8, where a long-living cloud of trapped particles is formed.

The role of particle feedback has been recently demonstrated in a similar system, where a vortex flow is created in a convective cell by imposing a temperature gradient across the side walls [59]. The particle feedback results in a significant suppression of the vortex flow, which leads to a cloud of smaller size. The reason is that the buoyancy convective flow is caused by small variations of density related to nonisothermality of the medium. If density variations due to nonuniformity of the particle distribution are comparable with those due to nonisothermality, particle feedback cannot be ignored. Technically, to account for feedback effects, one has

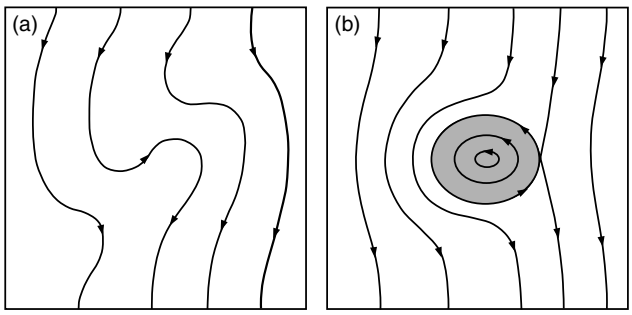

Figure 9. Sketch of streamlines of the particle flow, $\mathbf{v}$, in the absence (a) and in the case (b) of particle entrapment. The cloud of trapped particles is shaded darkly.

to consistently solve an equation for the velocity field, which becomes dependent on the concentration of particles, $C(\mathbf{r}, t)$. In our example, a feedback term appears in the equation for $\mathbf{v}$ and leads to effectively smaller buoyancy. More generally, the feedback term is proportional to the volume fraction C and an external force $\mathbf{F}$. Even if C is very small, the product $C\mathbf{F}$ is finite provided the force is large enough. As a result, this term is non-negligible in comparison with other forces. In the example of sedimenting particles, even for volume fractions of 1% the feedback term is of the same order as the buoyancy term responsible for convective flow. We stress that, as particles are widely used for visualization of flows, one has to keep in mind possible feedback effects, as otherwise this may lead to a wrong interpretation of measurements.

The described mechanism of particle entrapment neglects diffusion of particles, which is reasonable at macroscopic scales. For instance, for a fine spherical particle of size $a \simeq 0.1$ μm suspended in water at room temperature we obtain the diffusion coefficient $D \sim 10^{-8}$ cm^2 s^{-1}. The diffusion timescale $\tau_\mathrm{d} = L^2/D$ sets the typical time of existence of a cloud of trapped particles, which means that no proper particle entrapment can be achieved at times $t > \tau_\mathrm{d}$. For laboratory length scales, $L \sim 1$ cm, this is not a problem, as this time is very long, $\tau_\mathrm{d} \sim 10^8$ s. However, at microscales, $L \sim 1$ μm, the particles can be trapped for at most a few seconds, $\tau_\mathrm{d} \sim 1$ s. Thus, the conventional mechanism of entrapment can become inefficient at microscopic scales. We next describe how the particle feedback can be used to achieve particle entrapment at small scales.

Consider a suspension of small polarizable particles in a long closed microchannel. The particles are driven by the externally imposed dielectrophoretic (DEP) force [60]. The transverse component of the DEP force influences migration of the particles across the channel, which leads either to attraction (positive-DEP) or repulsion (negative-DEP) by the electrodes. The longitudinal component controls the particle transport along the channel. Because of the particle feedback, the particles cause the initially quiescent fluid to move, which eventually leads to a steady fluid flow with a profile with vanishing mean flux [74], shown in figure 10(a). In a real set-up only a part of the channel is covered by the electrodes. Away from the electrodes there is no source of motion, which results in a flow pattern in the form of large-scaled vortices, as

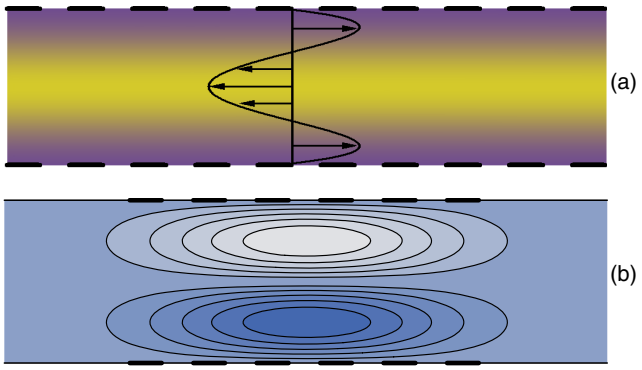

Figure 10. (a) Distribution of particles in a microchannel under traveling-wave (negative) DEP. The higher and lower values of the particle concentration correspond to lighter and darker domains, respectively. The traveling wave is imposed at the horizontal boundaries (electrode arrays are sketched with dashed lines), which leads to fluid motion with a nontrivial velocity profile via particle feedback. (b) Flow pattern in a typical DEP set-up. Lighter and darker colored vortices correspond to clockwise and counterclockwise rotation, respectively.

in figure 10(b). As the particles are involved in vortical motion, this mechanism is, in many ways, reminiscent of conventional particle entrapment.

However, there are two principal differences. First and most important, the conventional entrapment implies the existence of a vortex flow irrespective of whether there are any particles or not [72]. The fluid flow in the considered system can be induced by the particles only. In contrast to previous studies, particle entrapment arises as a generic particle feedback effect, which also provides a tool to generate a flow. Second, in contrast to the usual mechanism of entrapment in macroscopic vortex flows, which becomes unstable against diffusion at small scales, this particle-induced mechanism involves diffusion of particles as a necessary ingredient. The revealed effect resembles DEP experiments [75], where the similar formation of a pair of vortices in a microchannel accompanied by particle entrapment has been observed.

3.2. Bubbles as soft particles: collective dynamics and the role of particle feedback

The dynamics of single and multiple inclusions suspended in a liquid environment has been attracting much attention for many years [76]. Of special interest is a bubbly medium with bubbles as soft, deformable objects. Because of their compressibility, bubbles are able to exhibit an additional degree of freedom if compared with solid, nondeformable inclusions. One of the simplest examples of the system where this factor becomes of crucial importance is a bubbly liquid under high frequency oscillations.

The key feature in the dynamics of a single bubble is the existence of the breathing mode of eigenoscillations, which corresponds to volume oscillations (or radial pulsations) of the bubble. This type of dynamics is typical of compressible objects only: the bubble changes its volume without changing its shape [77]. Interaction of this mode with the translational motion, which takes place for any particle irrespective of the compressibility of the particle, is well known to cause an averaged force [78], leading to the effects of accumulation.

A well-known observation is the appearance of an averaged force on a single bubble suspended in the liquid under the action of an acoustic field [78–80]. The time-averaged force $\mathbf{F}_\mathrm{b}$ exerted on the bubble of equilibrium radius R in the standing wave of pressure $p = p_0(z)\cos\omega t$ is proportional to ∇p_0^2. For instance, in the particular case of $p_0(z) = P_0 \cos kz$ this force is given by

$$\mathbf{F}_\mathrm{b} = -\frac{\pi k R P_0^2}{\rho\omega^2\left(\Omega^2 - 1\right)} \sin(2kz)\mathbf{e}_z, \tag{21}$$

where ρ is the density of the liquid, ω is the frequency of external driving, $k = \omega/c_0$ is the wavenumber with c_0 being the speed of sound in the liquid free of bubbles and $\mathbf{e}_z$ is the unit vector along the z axis. The dimensionless parameter Ω represents the ratio of the eigenfrequency of volume oscillations [77, 81] to the external frequency ω.

As follows from expression (21), the bubble moves to the antinodes of the pressure wave at low frequency ω ($\Omega > 1$) and to the nodes at high frequency ω ($\Omega < 1$). This generic behavior is known as the primary Bjerknes effect and the averaged force as in equation (21) is referred to as the Bjerknes force.

The simplest way to obtain the averaged description of a bubbly liquid is to treat the bubbles in a superimposed acoustic field independent of each other, where each bubble in the field experiences the Bjerknes force, like in equation (21). Such a description, however, may lack in possible collective or feedback effects, as we already demonstrated for nondeformable particles in section 3.1. The averaged dynamics of bubbles coupled to the liquid ambient including the dynamics in confined geometries has received no proper theoretical attention. A step in this direction has been recently made in [69], where an averaged model of a dilute bubbly liquid including feedback effects is developed. The oscillations are assumed small amplitude and high frequency in the sense that

$$ah \ll R^2, \qquad \omega R^2 \gg \nu, \tag{22}$$

where a is the amplitude of oscillations, ν is the kinematic viscosity of liquid and h ($R \ll h$) is the typical length scale, see also figure 11. On the other hand, the frequency ω is chosen so small that no acoustic waves are possible in the medium without bubbles, $\omega h \ll c_0$. Note that the last point is in contrast with the system as described by equation (21). Here, the liquid remains incompressible and, without bubbles, moves as a solid body. All nontrivial effects come from the presence of bubbles, which ensure that the altogether medium is compressible.

The system is characterized by two considerably different timescales: the 'fast' oscillation time $1/\omega$ and the 'slow' dissipative timescale h^2/ν. This hierarchy of timescales makes it possible to treat the fast oscillatory and slow (averaged) motions separately. One performs the averaging over the fast

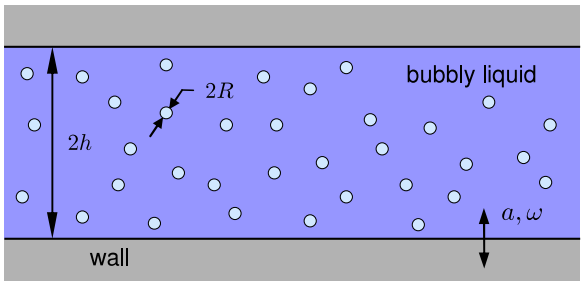

Figure 11. Sketch of a confined bubbly liquid subject to oscillations transverse to the walls.

timescale, obtains an expression for the averaged 'vibration' force and finally arrives at a closed self-consistent model describing averaged motion of a monodisperse bubbly liquid without [69] or with [71] the diffusivity of bubbles.

The developed theoretical models are applied to describe the dynamics of a confined bubbly liquid filling the space between two solid walls, figure 11. The initial state corresponds to motionless liquid and bubbles, with a uniform distribution of bubbles. Depending on the frequency ω, the bubbles can migrate towards the walls or accumulate in thin sheets parallel to the boundaries, which can be located exactly at the central plane or shifted away from the center towards the boundaries. This accumulation can lead to the formation of bubbly screens [82], when diffusion of bubbles is not important, or can lead to steady states for diffusive bubbles [71]. It has been shown that a bubbly liquid behaves similar to the primary Bjerknes effect: at relatively low frequencies ω ($\Omega > 1$) the bubbles leave the nodes and accumulate in the antinodes of the pressure wave, while at high frequencies ω ($\Omega < 1$) the bubbles migrate to the nodes. We stress that, in contrast to the case of a single bubble, the ensemble of bubbles significantly affects the vibration field and hence the characteristics of the liquid phase. Due to this feedback effect, the bubbles do not simply follow the externally superimposed nonuniform field, as in the conventional Bjerkness effect, but also create this nonuniformity.

3.3. Zigzag transition and explosions in colloidal chains

As mentioned in section 1, colloidal systems are relatively simple systems that allow for reliable experimental analysis and provide a possibility of comparison with theory and computer simulations [9]. Here, external forces can be widely used to drive nonequilibrium behavior. Recent examples include nonlinear instabilities in sedimenting suspensions [83], dynamic lane formation in oppositely charged particles under electric fields [84], driven dislocation nucleation [85] and stochastic resonance [86]. Further, we describe the ability to tune intercolloidal magnetic interactions through the application of an external magnetic field [87] while simultaneously trapping colloids in a line by using optical tweezers.

Experimentally, superparamagnetic colloidal particles are individually trapped by optical tweezers [88]. Application of external magnetic fields induces a dipolar repulsion between the colloids. Subsequently, removing the optical traps results in a colloidal explosion leading to zigzag pattern formation, see figure 12. Notably, we observe explosions with a zigzag pattern that persists even when magnetic interactions are much weaker than those that break the linear symmetry in equilibrium.

Theory and Brownian dynamics simulations can quantitatively describe the experimentally observed phenomenon both in and out of equilibrium [88]. As can be shown theoretically, there exists the transition from an equilibrium nonzigzag to a zigzag state, which is possible for certain traps only and occurs at a critical parameter that characterizes the ratio of optical and magnetic forces. A comparison of normal modes obtained experimentally and numerically, allows us to ascribe the explosion feature to the softening of the transverse normal mode band upon approaching the zigzag transition and show the dominance of the zigzag mode below the threshold point. An analysis of the mode spectrum can quantify the nonharmonic nature of the optical traps. More generally, the introduced methodology, where colloids are propelled in a well-controlled manner upon switching off an optical field, may be

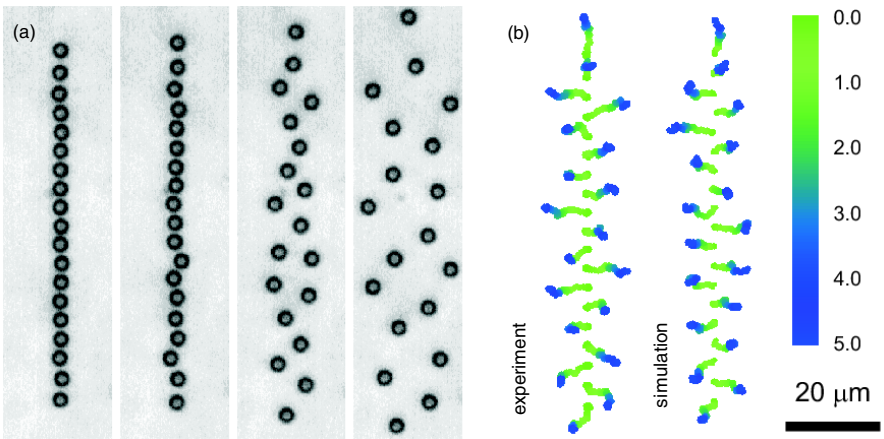

Figure 12. (a) Microscopy images showing an exploding one-dimensional array of 19 magnetic particles upon removing the optical traps. (b) The experimental and simulated particle trajectories of the exploding chain. The color code indicates the time in seconds.

applied to other geometries, with potential applications in microfluidics.

4. Wetting and contact line dynamics

Whereas oscillations of drops suspended in a fluid away from the boundaries have been studied for over a century [77, 78], oscillations of drops and bubbles in contact with solid surfaces have only received attention for the last few decades. Understanding fundamental aspects of drops and bubbles interacting with the solid surface is closely related to the problem of wetting. This knowledge is of practical importance because many technological processes deal with spreading of a liquid (a paint, a lubricant or a dye) over solid surfaces [15]. From the theoretical point of view, the presence of a solid surface often meets another problem, the contact line dynamics, which is currently far from being fully understood. Many theoretical efforts have been successfully put forth to attack slow (steady) motion of the contact line [15, 20], which is often very well described in the lubrication approximation [17]. However, neither rigorous theory nor satisfactory understanding exist for unsteady motion, especially for fast oscillatory processes.

As discussed in section 3.2, a compressible bubble suspended in an oscillating liquid medium exhibits nontrivial dynamics. A challenging question concerns the situation when the bubble comes close and sits on the boundary. Below we discuss what happens to a drop or a bubble in contact with the oscillating wall. Because the correct description of the interaction with boundaries is a crucial prerequisite for obtaining the proper picture of the bulk dynamics in confined systems, this problem is closely related to the systems as in section 3.2.

Another closely related problem underlying the physics of wetting concerns thin film instabilities. Here, the lubrication approximation provides an amplitude equation of Cahn–Hilliard type. A number of numerical studies [89–91] have shown film rupture leading to the formation of a cascade of 'drops' and 'fractal-like fingering' [19] comprising the gaps or 'dry spots' [89, 90] between the drops. These findings have been supported by direct simulations of the Navier–Stokes equations [92, 93]. We discuss how this long-standing problem is solved in section 4.2.

4.1. Sessile bubbles and droplets on an oscillating substrate

A number of important conclusions can be drawn from simplified geometries where analytical solutions can be obtained. Such examples refer, for instance, to a hemispherical liquid droplet (or a bubble) sitting on an oscillating substrate. Here one has to distinguish between the situations of incompressible and compressible objects.

To describe the contact line motion, a boundary condition that captures principal features of the contact line motion has been suggested by Hocking [22], see also figure 13:

$$\frac{\partial \zeta}{\partial t} = \begin{cases} \Lambda(\gamma - \gamma_c), & \gamma > \gamma_c, \\ 0, & |\gamma| \leqslant \gamma_c, \\ \Lambda(\gamma + \gamma_c), & \gamma < -\gamma_c, \end{cases} \tag{23}$$

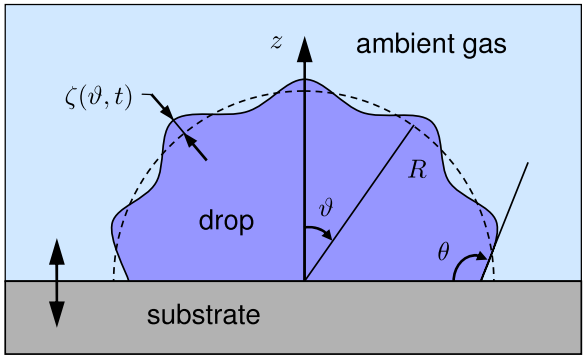

Figure 13. Typical problem geometry. A sessile hemispherical drop upon a transversally oscillating substrate.

where $\zeta(\vartheta, t)$ is the deflection of the interface, $\gamma = \theta - \theta_0$ is the deviation of the contact angle θ from its equilibrium value θ_0 and γ_c is a threshold value. The factor Λ, which has the dimension of velocity, characterizes the interaction between the substrate and the liquid and is referred to as the wetting or the Hocking coefficient. Condition (23) is able to correctly reproduce the contact angle hysteresis. It implies that the contact line starts to move only when the deviation of the contact angle exceeds a certain critical value.

In the important particular case $\gamma_c = 0$, in which the contact line velocity $\partial\zeta/\partial t \propto \gamma$, condition (23) describes no contact angle hysteresis [23] and for $\theta_0 = \pi/2$ can be approximated as

$$\frac{\partial \zeta}{\partial t} = \Lambda \mathbf{n} \cdot \nabla \zeta, \tag{24}$$

where $\mathbf{n}$ is the external normal to the solid surface.

Different practically important situations can be addressed by changing Λ or, in terms of the dimensionless wetting (or Hocking) parameter, $\lambda = \Lambda\sqrt{\rho R/\sigma}$. Here, R is the equilibrium radius of the droplet, ρ is the density of liquid and σ is the surface tension. Thus, different regimes range from the completely pinned contact line, $\lambda \to 0$ (the contact angle can change), to the opposite case of the fixed contact angle, $\lambda \to \infty$ (the contact line slides).

Based on the described approach we have first studied the dynamics of a sessile hemispherical bubble [25]. The contact line motion is taken into account by applying the Hocking boundary condition without hysteresis (24). On the other hand, the bubble is considered as a compressible object. One of the main messages is that it has been proven that the linear shape and volume oscillations demonstrate a clear interaction—contrary to the necessarily nonlinear coupling for a spherical bubble, see, for example, a survey by Feng and Leal [94]. However, the compressibility of the bubble leads to two peculiar effects. The spectrum of eigenfrequencies ω is determined by the equation [25]

$$\mathrm{i}\omega\left(\omega^2 \sum_{n=1}^{\infty} \frac{\alpha_n P_{2n}(0)}{\Omega_n^2 - \omega^2} - \frac{1}{2} - \frac{1}{\Omega_0^2 - \omega^2}\right) = \lambda, \tag{25}$$

$$\Omega_0^2 = \Pi_0 - 2, \qquad \Omega_n^2 = (2n-1)(2n+1)(2n+2) \qquad (n > 0) \tag{26}$$

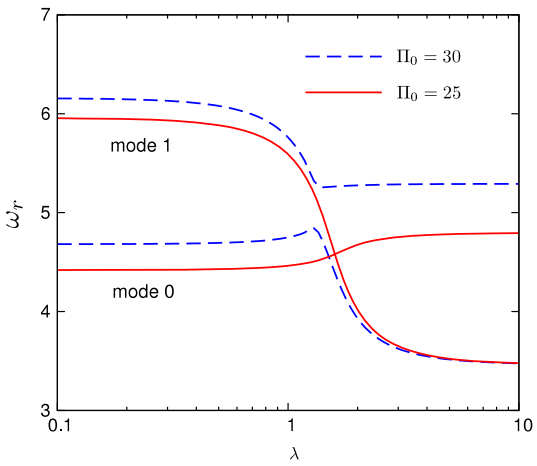

Figure 14. Rearrangement of two lowest modes, 0 and 1, under small variation of pressure Π_0. The real part of eigenfrequencies ω_r versus wetting parameter, λ.

and is dependent on an additional parameter, dimensionless pressure in the bubble Π_0. Here, P_n are Legendre polynomials, coefficients $\alpha_n = -(4n+1)P_{2n}(0)/[(2n-1)(2n+2)]$; Ω_0 and Ω_n ($n > 0$) are, respectively, the dimensionless frequency of the breathing mode and frequencies of the shape oscillations (for even modes) of a spherical bubble of the same radius. The frequencies are measured in units of $\sqrt{\sigma/(\rho R^3)}$.

Generally, equation (25) admits no analytical solution and has to be solved numerically. An analysis of the spectrum shows a nontrivial interaction of the volume and shape oscillations leading to a newly found rearrangement of branches in the spectrum, see figure 14. As a particular consequence of the rearrangement, the eigenfrequencies of the compressible bubble can not only monotonically decrease with λ, as in the case of the drop or incompressible bubble, but also monotonically grow.

The second feature caused by compressibility is a 'double resonance' taking place at a frequency of substrate oscillations $\Omega \approx \Omega_0 \approx \Omega_k$. Note that it is always possible for a compressible bubble to make the frequencies Ω_0 and Ω_k close, as the frequency of the breathing mode Ω_0 can be tuned via the parameter Π_0, see equation (26). The existence of this resonance follows directly from the problem of natural oscillations, where the specific case $\Omega_0 = \Omega_k$ predicts no damping of oscillations. As can be shown [25], there always exists an eigenfrequency ω_{0k} of the hemispherical bubble

$$\omega_{0k} = \frac{\gamma_0\Omega_k}{\gamma_0+\gamma_k} + \frac{\gamma_k\Omega_0}{\gamma_0+\gamma_k}, \tag{27}$$

which is between Ω_0 and Ω_k. Here, $\gamma_0 = 1/2$ and $\gamma_k = -\Omega_k^2\alpha_k P_{2k}(0)/2$ ($k > 0$). The damping of natural oscillations $\simeq\delta^2$ with $\delta = (\Omega_0^2 - \Omega_k^2)/\Omega_k^2$. As a result, the forced oscillations at $\Omega \approx \Omega_0 \approx \Omega_k$ turn out to be resonant; the amplitude of resonant oscillations is

$$A_{\rm res} = \frac{\Omega_k}{\lambda}\left(\frac{\gamma_0+\gamma_k}{\gamma_0}\right)^2\delta^{-2}, \tag{28}$$

which is achieved at $\Omega = \omega_{0k}$.

A similar study concerns the dynamics of an oscillated sessile droplet of incompressible liquid (figure 13) with the focus on the contact angle hysteresis [95]. To take into consideration the contact angle hysteresis, the boundary condition in the form (23) is applied. Because the contact line is able to move only when the deviation of the contact angle exceeds a certain critical value the stick–slip dynamics is observed: the system switches periodically between the states with the sliding and the fixed contact line. We detect two major effects caused by the contact angle hysteresis.

It is known that, in the nonhysteretic limit [24], $\gamma_0 = 0$, no contact line motion exists at a certain number of discrete frequencies $\Omega = \Omega_{\rm ar}$, which are independent of the wetting parameter. For this reason, the values $\Omega_{\rm ar}$ are referred to as antiresonant frequencies. We have shown that the contact angle hysteresis, when $\gamma_0 \neq 0$, transforms this discrete number of frequencies into antiresonant frequency bands of finite width [95]. With the growth of γ_0, the parameter domains of the stick–slip dynamics become narrower, whereas the one with the completely fixed contact line grows. Another effect caused by contact angle hysteresis is that the time dependence of contact angle, $\gamma(t)$, displays a nontrivial behavior. Compared with the case of no hysteresis, the dependence $\gamma(t)$ shows a more complicated behavior reminiscent of recent experimental observations [27]. This feature can be consistently explained by competing resonances.

4.2. Formation of a cascade of sessile droplets

To address the problem of fractal fingering, we first relate liquid droplets with zero contact angle to dissipative compactons [96]. A usual compacton is a well-known compact (i.e. with finite support) traveling-wave solution, which emerges in conservative systems with nonlinear dispersion [97, 98]. We show that its stationary analog with compact support naturally appears in dissipative systems with nonlinear dissipation and, therefore, can be referred to as a stationary 'dissipative compacton' (DC). Second, we demonstrate that a DC presents a primitive element mediating the formation of hierarchical fractal structure and characterize the fractal properties of this structure quantitatively. Remarkably, in conservative systems a hierarchy of compactons also evolves from initial data, but they all move away; contrary to this, DCs do not move, thus arranging a fractal.

Consider a one-dimensional Cahn–Hilliard equation describing dissipative evolution of a conserved field $h(x,t)$:

$$\frac{\partial h}{\partial t} + (h^2 h_x + h^3 h_{xxx})_x = 0. \tag{29}$$

Note that equation (29) describes the dynamics of a thin film over a substrate heated from below in the limit of small h, where h plays the role of local thickness. This equation admits a stationary compact solution $h = H(x)$ in the form of a DC or a 'touchdown steady state' [99], nonvanishing for $|x| \leqslant l$ only:

$$x = \pm\sqrt{\pi\mathcal{H}}\,\mathrm{erf}\left(\sqrt{\frac{1}{2}\ln\frac{\mathcal{H}}{H}}\right), \qquad \mathcal{H} = \max_x H(x), \tag{30}$$

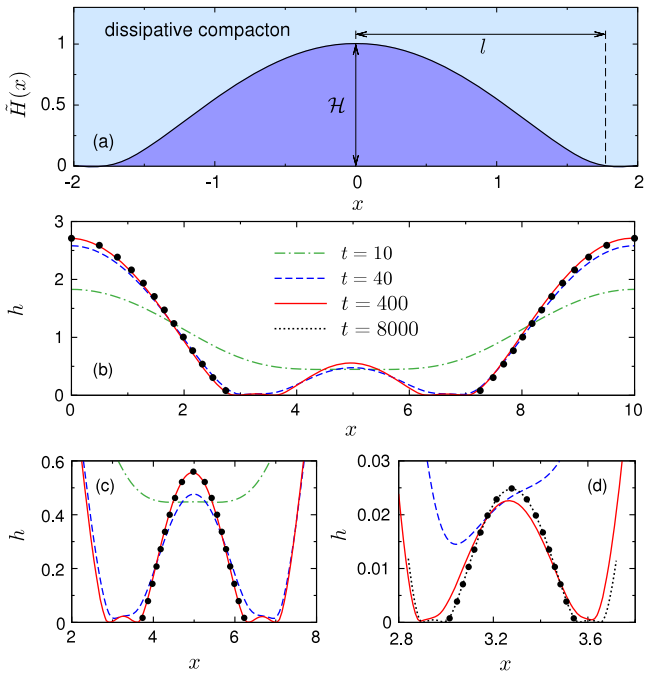

Figure 15. The profile of the base DC, $\tilde{H}(x)$, according to equation (30) (a). Evolution of the field $h(x, t)$ illustrating hierarchical formation of droplets, $d = 10$. (b) Snapshots of h. Panels (c) and (d) are zoomed-in fragments of panel (b). Lines represent numerical results for equation (29), while circles show the profiles of corresponding DCs as in equation (30).

where $\mathrm{erf}(z) = \sqrt{2/\pi}\int_0^z \mathrm{e}^{-t^2}\,\mathrm{d}t$. Solution (30) represents a self-affine one-parameter family of DCs parametrized by $\mathcal{H}$ and expressed in terms of the base DC $\tilde{H}(x)$ having $\mathcal{H} = 1$, figure 15(a):

$$H(x) = \mathcal{H}\tilde{H}(x/\sqrt{\mathcal{H}}), \qquad l = \sqrt{\pi\mathcal{H}}. \tag{31}$$

For a thin film, the DC describes the stationary profile of a drop with the height $\mathcal{H}$ and zero contact angle. The property of self-affinity is a necessary prerequisite for the emergence of the fractal structure of droplets described by equation (29). The results of stability analysis and direct numerical simulation of equation (29) show that the solution in the form of a DC is stable against perturbations of zero volume. For perturbations of nonzero volume, the DC turns out to be unstable. Here we detect a breakup of the DC with the emergence of a complex structure.

We now demonstrate numerically the formation of a fractal, hierarchical structure of DCs. Equation (29) is solved numerically in the computation domain $x \in [0, d]$ with periodic boundary conditions. A distorted uniform profile $h(x, t = 0) = 1 + 0.1\cos(2\pi x/d)$ is chosen as an initial condition. An example of computations is presented in figures 15(b) and (c). There we also compare the numerically obtained profile $h(x)$ having local maxima $h_{\mathrm{m}}^{(n)}$, $n = 1, 2, \ldots$ with the DC profiles with $\mathcal{H} = h_{\mathrm{m}}^{(n)}$, denoted as $\mathrm{DC}^{(n)}$. We see that the initial profile develops into a hierarchical structure of DCs of different amplitudes.

The observed structure along with the property of self-affinity suggest that the formation of higher-order DCs never stops and the dry spots between DCs form a fractal reminiscent of the Cantor set. Thus, a DC plays a role of an 'intrinsic mode', inherent in the fractalization. Moreover, this fractal can be characterized quantitatively. It can be shown that the variation of L_n, the distance between the neighboring DCs of nth and $(n-1)$th orders, versus the base $2l_n$ of $\mathrm{DC}^{(n)}$ obeys a power law:

$$L_n \approx \alpha\,(2l_n)^{\beta}, \qquad \alpha \approx 0.2, \quad \beta \approx 1.25. \tag{32}$$

Because $\beta > 1$ in equation (32), with the increase in n the ratio L_n/l_n diminishes, implying that the smaller daughter DCs tend to occupy the whole space between their bigger parent DCs. The fraction of dry spots tends to zero and, therefore, the fractal dimension of this set equals zero. Furthermore, for large n we can neglect the distance between $\mathrm{DC}^{(n)}$ and $\mathrm{DC}^{(n+1)}$ and put $L_n \approx 2l_{n+1}$. As a result, equation (32) entails a remarkable superexponential scaling of l_n with n: $\log(l_n) \propto \beta^n \log(l_0)$.

Thus, as a result of rupture, the thin film evolves into a hierarchical structure of droplets. The fact that all the droplets can be represented by the DCs of different amplitudes is a key point in understanding the fractalization process. The precise knowledge of the DC properties, as an intrinsic mode of the structure, allows us to draw several crucial conclusions providing the solution to the long-standing problem of fractal-like fingering [19]. The fractal is characterized by superexponentially decreasing amplitudes and lengths. The complementary set built of dry spots between the DCs has zero dimension. It is noteworthy that, in contrast to widespread random fractals, the revealed fractal is a regular one. In this way it is similar to a recent example of an exact, soliton-based fractal in nonlinear optics [100], but with a compact basic mode.

We also emphasize that the DC is, in many ways, similar to the conservative compacton (like dissipative solitons that share many properties with conservative solitons). In both cases, an initial profile splits into a hierarchy of self-similar objects: traveling compactons [97, 98] or stationary DCs [96]. In the latter case the DCs arrange themselves forming a fractal. We expect this property not only for the class of Cahn–Hilliard equations (29) considered, but for general models possessing self-affine DCs.

Acknowledgments

I would like to acknowledge a number of coauthors who contributed to different parts of the presented results: A Pikovsky, S Shklyaev, M Abel, I Fayzrakhmanova, D Lyubimov, T Lyubimova, A Louis, J Baumgartl, C Bechinger and R Dullens. I would also like to thank K Jacobs and F Müller for providing a fruitful and stimulating environment within Priority Program SPP 1164 'Nano- and Microfluidics' by the German Science Foundation (DFG). The financial support under grant nos. STR 1021/1-1 and STR 1021/1-2 is gratefully acknowledged.

References

[1] Ho C M and Tai Y C 1998 *Annu. Rev. Fluid Mech.* **30** 579
[2] Nguyen N-T and Wereley S T 2002 *Fundamentals and Applications of Microfluidics* (Boston, MA: Artech House)

[3] Eijkel J C T and van den Berg A 2005 *Microfluidics Nanofluidics* **1** 249
[4] Whitesides G M 2006 *Nature* **442** 368
[5] Squires T M and Quake S R 2005 *Rev. Mod. Phys.* **77** 977
[6] Manghi M, Schlagberger X, Kim Y-W and Netz R R 2006 *Soft Matter* **2** 653
[7] Kapral R 2008 *Adv. Chem. Phys.* **140** 89
[8] Gompper G, Ihle T, Kroll D M and Wrinkler R G 2009 *Adv. Polym. Sci.* **221** 1
[9] Löwen H 2001 *J. Phys.: Condens. Matter* **13** R415
[10] Kim A and Karrila S J 1991 *Microhydrodynamics: Principles And Selected Applications* (Boston, MA: Butterworth–Heinemann)
[11] Russel W B, Saville D A and Schowalter W R 1989 *Colloidal Dispersions* (Melbourne: Cambridge University Press)
[12] Dhont J K G 1996 *An Introduction to Dynamics of Colloids* (Amsterdam: Elsevier)
[13] Tuinier R and Taniguchi T 2005 *J. Phys.: Condens. Matter* **17** L9
[14] Israelachvili J N 1994 *Intermolecular and Surface Forces* (London: Academic)
[15] de Gennes P-G 1985 *Rev. Mod. Phys.* **57** 827
[16] Rauscher M and Dietrich S 2008 *Annu. Rev. Mater. Res.* **38** 143
[17] Oron A, Davis S H and Bankoff S G 1997 *Rev. Mod. Phys.* **69** 931
[18] Craster R V and Matar O K 2009 *Rev. Mod. Phys.* **81** 1131
[19] Yeo L Y, Craster R V and Matar O K 2003 *Phys. Rev.* E **67** 056315
[20] Pismen L M and Thiele U 2006 *Phys. Fluids* **18** 042104
[21] Dussan V E B 1979 *Annu. Rev. Fluid Mech.* **11** 371
[22] Hocking L M 1987 *J. Fluid Mech.* **179** 267
[23] Hocking L M 1987 *J. Fluid Mech.* **179** 253
[24] Lyubimov D V, Lyubimova T P and Shklyaev S V 2006 *Phys. Fluids* **17** 012101
[25] Shklyaev S and Straube A V 2008 *Phys. Fluids* **20** 052102
[26] Dong L, Chaudhury A and Chaudhury M K 2006 *Eur. Phys. J.* E **21** 231
[27] Noblin X, Buguin A and Brochard-Wyart F 2004 *Eur. Phys. J.* E **14** 39
[28] Daniel S, Chaudhury M K and de Gennes P-G 2005 *Langmuir* **21** 4240
[29] Cross M C and Hohenberg P C 1993 *Rev. Mod. Phys.* **65** 851
[30] Abraham E R 1998 *Nature* **391** 577
[31] Huisman J, Thi N N P, Karl D M and Sommeijer B 2006 *Nature* **439** 322
[32] Leconte M, Martin J, Rakotomalala N and Salin D 2003 *Phys. Rev. Lett.* **90** 128302
[33] Neufeld Z, López C, Hernández-García E and Piro O 2002 *Phys. Rev.* E **66** 066208
[34] Tél T, de Moura A, Grebogi C and Károlyi G 2005 *Phys. Rep.* **413** 91
[35] Aref H 1984 *J. Fluid Mech.* **143** 1
[36] Ottino J M 1989 *The Kinematics of Mixing: Stretching, Chaos, and Transport* (Cambridge: Cambridge University Press)
[37] Aref H 2002 *Phys. Fluids* **14** 1315
[38] Rothstein D, Henry E and Gollub J P 1999 *Nature* **401** 770
[39] Antonsen T M, Fan Z, Ott E and Garcia-Lopez E 1996 *Phys. Fluids* **8** 3094
[40] Pierrehumbert R T 1994 *Chaos, Solitons Fractals* **4** 1091
[41] Pikovsky A and Popovych O 2003 *Europhys. Lett.* **61** 625
[42] Straube A V, Abel M and Pikovsky A 2004 *Phys. Rev. Lett.* **93** 174501
[43] Pikovsky A S 1984 *Z. Phys.* **B 55** 149
[44] Pikovsky A S 1992 *Phys. Lett.* A **168** 276
[45] Nicolis G and Prigogine G 1977 *Self-Organization in Nonequilibrium Systems: From Dissipative Structures to Order Through Fluctuations* (New York: Wiley)
[46] Vasquez D A 2004 *Phys. Rev. Lett.* **93** 104501
[47] Turing A M 1952 *Phil. Trans. R. Soc.* B **237** 37
[48] Straube A V and Pikovsky A 2011 *Math. Modelling Nat. Phenom.* **6** 138
[49] Pismen L 2006 *Patterns and Interfaces in Dissipative Dynamics* (Berlin: Springer)
[50] van Saarloos W 2003 *Phys. Rep.* **386** 29
[51] Kuznetsov S P, Mosekilde E, Dewel G and Borckmans P 1997 *J. Chem. Phys.* **106** 7609
[52] McGraw P N and Menzinger M 2003 *Phys. Rev.* E **68** 066122
[53] Sibly R M, Barker D, Denham M C, Hone J and Pagel M 2005 *Science* **309** 607
[54] Murray J D 1993 *Mathematical Biology* (Berlin: Springer)
[55] Perlekar P, Benzi R, Nelson D R and Toschi F 2010 *Phys. Rev. Lett.* **105** 144501
[56] Straube A V and Pikovsky A 2007 *Phys. Rev. Lett.* **99** 184503
[57] Straube A V and Pikovsky A 2008 *Phys. Scr.* **T132** 014035
[58] Dimotakis P E 2005 *Annu. Rev. Fluid Mech.* **37** 329
[59] Lyubimov D V, Straube A V and Lyubimova T P 2005 *Phys. Fluids* **17** 063302
[60] Morgan H and Green N G 2003 *AC Electrokinetics: Colloids and Nanoparticles* (Baldock, Hertfordshire: Research Studies Press)
[61] Gijs M A M 2004 *Microfluidics Nanofluidics* **1** 22
[62] Snezhko A, Aranson I and Kwok W 2006 *Phys. Rev. Lett.* **96** 078701
[63] Belkin M, Glatz A, Snezhko A, Aranson I and Kwok W 2010 *Phys. Rev.* E **82** 015301(R)
[64] Hawkes J J, Cefai J J, Barrow D A, Coakley W T and Briarty L G 1998 *J. Phys. D: Appl. Phys.* **31** 1673
[65] Grier D G 2003 *Nature* **424** 810
[66] Terray A, Oakey J and Marr D W M 2002 *Science* **296** 1841
[67] Bleil S, Marr D W M and Bechinger C 2006 *Appl. Phys. Lett.* **88** 263515
[68] McWhirter J L, Noguchi H and Gompper G 2009 *Proc. Natl Acad. Sci. USA* **106** 6039
[69] Straube A V, Lyubimov D V and Shklyaev S V 2006 *Phys. Fluids* **18** 053303
[70] Kobelev Yu A and Ostrovsky L A 1989 *J. Acoust. Soc. Am.* **85** 621
[71] Shklyaev S and Straube A V 2009 *Phys. Fluids* **21** 063303
[72] Stommel H 1949 *J. Mar. Res.* **8** 24
[73] Maxey M R 1990 *Phil. Trans. R. Soc.* A **333** 289
[74] Shklyaev S and Straube A V 2008 *New J. Phys.* **10** 063030
[75] Felten M, Staroske W, Jäger M, Schwille P and Duschl C 2008 *Electrophoresis* **29** 2987
[76] Zapryanov Z and Tabakova S 1999 *Dynamics of Bubbles, Drops and Rigid Particles* (Dordrecht: Kluwer)
[77] Rayleigh L 1917 *Phil. Mag.* **34** 94
[78] Bjerknes V F K 1906 *Fields of Force* (New York: Columbia University Press)
[79] Blake F G 1949 *J. Acoust. Soc. Am.* **21** 551
[80] Eller A I 1968 *J. Acoust. Soc. Am.* **43** 170
[81] Minnaert M 1933 *Phil. Mag.* **16** 235
[82] Shklyaev S and Straube A V 2010 *Phys. Rev.* E **81** 016321
[83] Wysocki A, Royall C P, Winkler R G, Gompper G, Tanaka H, van Blaaderen A and Löwen H 2009 *Soft Matter* **5** 1340
[84] Leunissen M E, Christova C G, Hynninen A-P, Royall C P, Campbell A I, Imhof I, Dijkstra M, van Roij R and van Blaaderen A 2005 *Nature* **437** 235
[85] Schall P, Cohen I, Weitz D A and Spaepen F 2006 *Nature* **440** 319

[86] Babič D, Schmitt C, Poberaj I and Bechinger C 2004 *Europhys. Lett.* **67** 158
[87] Bubeck R, Bechinger C, Neser S and Leiderer P 1999 *Phys. Rev. Lett.* **82** 3364
[88] Straube A V, Louis A A, Baumgartl J, Bechinger C and Dullens R P A 2010 arXiv:1009.1930
[89] VanHook S J, Schatz M F, Swift J B, McCormick W D and Swinney H L 1995 *J. Fluid Mech.* **345** 45
[90] VanHook S J, Schatz M F, McCormick W D, Swift J B and Swinney H L 1997 *Phys. Rev. Lett.* **75** 4397
[91] Oron A 2000 *Phys. Fluids* **12** 1633
[92] Krishnamoorthy S, Ramaswamy S B and Joo S W 1995 *Phys. Fluids* **7** 2291
[93] Boos W and Thess A 1999 *Phys. Fluids* **11** 1484
[94] Feng Z C and Leal L G 1997 *Annu. Rev. Fluid Mech.* **29** 201
[95] Fayzrakhmanova I S and Straube A V 2009 *Phys. Fluids* **21** 072104
[96] Shklyaev S, Straube A V and Pikovsky A 2010 *Phys. Rev.* E **82** 020601(R)
[97] Rosenau P and Hyman J M 1993 *Phys. Rev. Lett.* **70** 564
[98] Rosenau P 1994 *Phys. Rev. Lett.* **73** 1737
[99] Laugesen R S and Pugh M C 2000 *Eur. J. Appl. Math.* **11** 293
[100] Sears S, Soljacic M, Segev M, Krylov D and Bergman K 2000 *Phys. Rev. Lett.* **84** 1902